BIOLOGICAL CRYSTALLOGRAPHY

ISSN 1399-0047

Structure of shikimate kinase, an *in vivo* essential metabolic enzyme in the nosocomial pathogen *Acinetobacter baumannii*, in complex with shikimate

Kristin A. Sutton,[a] Jennifer Breen,[a] Ulrike MacDonald,[b] Janet M. Beanan,[b] Ruth Olson,[b] Thomas A. Russo,[b,c] L. Wayne Schultz[a,d]‡ and Timothy C. Umland[a,d]*

[a]Hauptman–Woodward Medical Research Institute, Buffalo, NY 14203, USA, [b]Department of Medicine and The Witebsky Center for Microbial Pathogenesis, University at Buffalo, State University of New York, Buffalo, NY 14214, USA, [c]Veterans Administration Western New York Healthcare System and Department of Microbiology and Immunology, University at Buffalo, State University of New York, Buffalo, NY 14214, USA, and [d]Department of Structural Biology, University at Buffalo, State University of New York, Buffalo, NY 14203, USA. *Correspondence e-mail: umland@hwi.buffalo.edu

Received 14 April 2015
Accepted 22 June 2015

Edited by J. L. Martin, University of Queensland, Australia

‡ Present address: QuaDPharma, 11342 Main Street, Clarence, NY 14031, USA.

Keywords: shikimate kinase; *Acinetobacter baumannii*; essential gene; antibiotic target; multi-drug and extreme drug resistance; ligand-induced conformational change; enzyme kinetics.

PDB reference: shikimate kinase, complex with shikimate and sulfate ion, 4y0a

Supporting information: this article has supporting information at journals.iucr.org/d

Acinetobacter baumannii is an opportunistic Gram-negative pathogen that is an important cause of healthcare-associated infections exhibiting high mortality rates. Clinical isolates of multidrug-resistant (MDR) and extremely drug-resistant (XDR) *A. baumannii* strains are increasingly being observed. Compounding this concern is the dearth of new antibacterial agents in late-stage development that are effective against MDR and XDR *A. baumannii*. As part of an effort to address these concerns, two genes (*aroA* and *aroC*) of the shikimate pathway have previously been determined to be essential for the growth and survival of *A. baumannii* during host infection (*i.e.* to be essential *in vivo*). This study expands upon these results by demonstrating that the *A. baumannii aroK* gene, encoding shikimate kinase (SK), is also essential *in vivo* in a rat soft-tissue infection model. The crystal structure of *A. baumannii* SK in complex with the substrate shikimate and a sulfate ion that mimics the binding interactions expected for the β-phosphate of ATP was then determined to 1.91 Å resolution and the enzyme kinetics were characterized. The flexible shikimate-binding domain and LID region are compared with the analogous regions in other SK crystal structures. The impact of structural differences and sequence divergence between SKs from pathogenic bacteria that may influence antibiotic-development efforts is discussed.

1. Introduction

We are currently at risk of entering a 'post-antibiotic' era. Antibiotic resistance is increasing in both Gram-positive and Gram-negative bacteria, as exemplified by the clinically important microbes termed ESKAPE pathogens (Boucher *et al.*, 2013). *Acinetobacter baumannii* is one such pathogen, with growing incidences of multidrug-resistant (MDR) and extremely drug-resistant (XDR) strains. Mortality rates of >50% have been reported for infection by carbapenem-resistant *A. baumannii* strains (Spellberg & Bonomo, 2014; Lee *et al.*, 2014). The need for new antibiotic classes is acute (Perros, 2015), and their development holds the promise of increased durability since new classes may be less affected by existing resistance mechanisms. A desirable characteristic of an antibacterial target is *in vivo* essentiality (*i.e.* it is required for pathogen survival and growth during infection of a relevant host). Importantly, genes that are observed to be essential for pathogen growth on rich laboratory media may not be essential *in vivo* (Brinster *et al.*, 2009, 2010), or promising

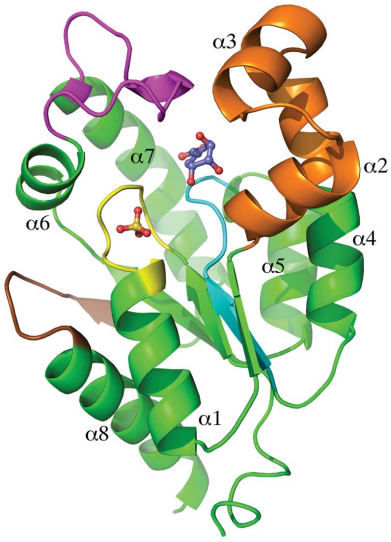

antibiotic targets may be overlooked if the *in vivo* environment is not considered (Fahnoe *et al.*, 2012). Our group has developed a genetic screen that efficiently identified putative *in vivo* essential *A. baumannii* genes, with a subset established as *in vivo* essential by assessing the growth and survival of isogenic mutant derivatives in a rat soft-tissue infection model (Umland *et al.*, 2012; Russo *et al.*, 2009, 2010). Two of the *A. baumannii* genes that were identified were *aroA* and *aroC*, which encode the successive enzymes 3-phosphoshikimate 1-carboxyvinyltransferase [PSCVT; alternate name 5-enolpyruvyl-shikimate 3-phosphate (EPSP) synthase] and chorismate synthase (CS), respectively, within the seven-step shikimate pathway (Umland *et al.*, 2012). The shikimate pathway is present in bacteria, fungi, apicomplexan parasites and plants, with the product chorismate serving as a precursor of aromatic amino acids and other aromatic metabolites, including folate, ubiquinone and vitamin K (Abell, 1999; Bentley & Haslam, 1990; Haslam, 1974; Herrmann & Weaver, 1999; McConkey *et al.*, 2004). Notably, this metabolic pathway is absent in humans. Inhibition of the shikimate pathway is the basis of the widely used herbicide glyphosate, which targets PSCVT in plants (Steinrücken & Amrhein, 1980) and exhibits *in vitro* activity against *Plasmodium falciparum* (McLeod *et al.*, 1998) and *Escherichia coli* (Rogers *et al.*, 1983). The shikimate pathway is a validated target for the development of new antimicrobial, antiparasitic and herbicidal agents (Coggins *et al.*, 2003).

Our *in vivo* essentiality screen did not saturate the *A. baumannii* genome. Hence, it was postulated that additional genes encoding upstream shikimate-pathway enzymes in *A. baumannii* may be also essential *in vivo* and thus should be evaluated as potential antibacterial targets. Shikimate kinase (SK) catalyzes the fifth step of the shikimate pathway, converting shikimate to shikimate 3-phosphate using ATP as a co-substrate, and is immediately upstream of PSCVT and CS. The respective substrate of each of these three enzymes shares a similar scaffold, suggesting that it may be possible to develop a multi-target antibiotic active against more than one enzyme of the pathway (Hsu *et al.*, 2013). This strategy will significantly decrease the likelihood of the evolution of resistance to such an agent. A site-directed Δ*aroK* mutant *A. baumannii* strain deficient in SK activity was constructed to verify *aroK* as *in vivo* essential using a rat soft-tissue infection model. As part of the next steps in logical antimicrobial development, *A. baumannii* shikimate kinase (abSK) was then structurally and kinetically characterized.

The crystal structure of abSK in complex with shikimate and a sulfate ion (SO_4^{2-}) that mimics the binding interactions expected for the β-phosphate of ATP was determined. abSK exhibits significant sequence diversity compared with the SK crystal structures currently deposited in the PDB, representing a total of nine homologs (eight from prokaryotes and one from Plantae). *E. coli* SK I (ecSK I) is the closest neighbor, with 54% sequence identity over 88% coverage. The remaining SK PDB entries range from 30 to 45% sequence identity to abSK. Comparison of abSK with these nine SK homologs reveals only 16 fully conserved residues and 19 additional highly conserved residues (8.5 and 10% of the 189 residues of abSK, respectively; Supplementary Fig. S1). abSK exhibits the fold characteristic of SKs and of nucleoside monophosphate kinases in general. However, even modest sequence and the resulting conformational differences may have significant consequences for antibiotic drug development against bacterial pathogen SKs, especially in the context of the induced-fit conformational changes that are typical within the SK family.

2. Materials and methods

2.1. Bacterial strains and growth medium

A. baumannii strain 307-0294 (AB307-0294) is a drug-susceptible clinical blood isolate selected as our model strain (Adams *et al.*, 2008; Umland *et al.*, 2012). A site-directed SK mutant (AB307Δ*aroK*) was constructed by allelic exchange of the majority of the target gene with a kanamycin-resistance gene in AB307-0294 as described by Luke *et al.* (2004). The construct was confirmed by sequence analysis of PCR-generated amplicons using primers outside of *aroK* (forward, 5′-AGGCGGAAGAAGAAGAAG-3′; reverse, 5′-TGTGATAAATCTGCCGCC-3′). The growth of AB307-0294 and AB307Δ*aroK* was assessed in rich laboratory medium (Luria–Bertani) through the measurement of the optical density at 600 nm over time (Russo *et al.*, 2009). All strains were maintained at 193 K in 50% LB broth and 50% glycerol prior to use.

2.2. Rat soft-tissue infection model

The *in vivo* essentiality of AB307-0294 *aroK* was evaluated using an established rat soft-tissue infection model. This infection model, approved by the University at Buffalo and the Veterans Administration Institutional Animal Care Committee, was conducted as reported previously (Russo *et al.*, 2010). The mean starting inocula for both AB307-0294 (wild type) and AB307Δ*aroK* were such as to result in 1.8×10^5 CFU ml^{-1}. The experiment was conducted using four replicates per *A. baumannii* strain, and *in vivo* bacterial growth and survival was quantitated at 1 min and 6, 24 and 48 h post-inoculation.

2.3. Recombinant protein expression and purification

E. coli strain DH5α (Invitrogen) was used during construction of the *aroK* expression vector, and strain Rosetta (DE3) (Novagen) was used for recombinant protein expression. PCR amplification of the complete *aroK* open-reading frame (NCBI ACJ56589) from purified AB307-0294 chromosomal DNA (RefSeq NC_011595.1) was accomplished using the primers forward, 5′-CGCCCGCATATGAAAGCAATTGAAAT-3′, and reverse, 5′-CGCGCGGCTCGAGCTATTTTAACTTG-3′, which included an NdeI and an XhoI cleavage site, respectively. Gel-purified PCR products were restriction-enzyme digested and ligated using T4 DNA ligase (Promega) into a linearized customized pETDuet vector (Novagen) containing an N-terminal His_6-SUMO affinity tag plus an Ulp1

protease cleavage site (pETDuet-SUMO-*aroK*). The integrity of the expression cassette was verified by DNA sequencing (Roswell Park Cancer Institute Sequencing Facility).

E. coli Rosetta (DE3) cells transformed with pETDuet-SUMO-*aroK* were grown to an OD_{600} of 0.8 at 310 K in Terrific Broth medium supplemented with 100 µg ml^{-1} ampicillin and 34 µg ml^{-1} chloramphenicol. The temperature was reduced to 289 K and protein expression was induced with 1 m*M* β-D-1-thiogalactopyranoside (IPTG). The culture was incubated for an additional 14 h prior to harvesting by centrifugation. Frozen cell pellets were thawed and resuspended in lysis buffer (50 m*M* Tris–HCl pH 7.5, 300 m*M* NaCl, 20 m*M* KCl, 5 m*M* $MgCl_2$, 0.5 m*M* DTT, 20 m*M* imidazole) plus 1 ml protease-inhibitor cocktail (Sigma–Aldrich) per litre of buffer. Cells were lysed *via* the addition of hen egg-white lysozyme to 1 mg ml^{-1} followed by processing using a microfluidizer (Microfluidics). The filtered lysate supernatant was loaded onto a HisTrap immobilized metal-ion affinity chromatography (IMAC) column (GE) and eluted with lysis buffer plus 300 m*M* imidazole. Elution fractions containing His_6-SUMO-abSK were dialyzed into lysis buffer, and Ulp1 protease was added to the fusion protein at a 1:150 mass ratio and incubated overnight at 4°C (Mossessova & Lima, 2000). The sample was reapplied onto a HisTrap IMAC column to separate the cleaved His_6-SUMO affinity tag from abSK. Size-exclusion chromatography (SEC) using a HiLoad 16/60 Superdex 75 column (GE) was performed as a final polishing step using an elution buffer consisting of 50 m*M* Tris–HCl pH 7.5, 300 m*M* NaCl, 20 m*M* KCl, 5 m*M* $MgCl_2$, 0.5 m*M* DTT. The eluted abSK was dialyzed into 25 m*M* Tris–HCl pH 7.5, 0.5 m*M* DTT. Purified abSK at ∼1 mg ml^{-1} was flash-frozen in liquid nitrogen in small aliquots and stored at 193 K. Protein purity was verified *via* SDS–PAGE.

2.4. Shikimate kinase kinetics

The enzymatic activity of abSK was determined using an assay that couples the release of ADP to pyruvate kinase (PK) and lactate dehydrogenase (LDH) reactions (Millar *et al.*, 1986; Rosado *et al.*, 2013). The shikimate-dependent decrease in absorbance owing to the oxidation of NADH was monitored at 340 nm at 15 s intervals. Assays were conducted at 298 K in 96-well polystyrene flat-bottom plates (Costar) with a BioTek Synergy 4 plate reader. The assay solution (total volume 200 µl) consisted of 100 m*M* Tris–HCl pH 7.5, 100 m*M* KCl, 1.2 m*M* ATP, 5 m*M* $MgCl_2$, 1.5 m*M* phosphoenolpyruvate, 0.2 m*M* NADH, 6 U ml^{-1} PK and 5 U ml^{-1} LDH. The reaction was initiated by the addition of purified abSK to a final concentration of 50 n*M*. Kinetic parameters were determined from initial velocity measurements at varying concentrations of shikimate (10–1200 µ*M*). The final kinetic parameters were calculated by nonlinear regression analysis using the enzyme-kinetics module of *GraphPad Prism* (GraphPad Software Inc.). The assays were performed in triplicate.

2.5. Crystallization

Shikimate and ADP were added to a concentration of 2.5 m*M* each, and $MgCl_2$ was added to 10 m*M*, prior to protein concentration (to a final concentration of 15 mg ml^{-1} as determined by the Bradford method) using Centricon-10 centrifugal concentrators (Amicon). Crystallization screening *via* microbatch-under-oil in 1536-well microtitre plates was conducted using the high-throughput robotics at the Hauptman–Woodward Institute (Luft *et al.*, 2003). Conditions were optimized *via* manual sitting-drop vapor diffusion, mixing 3 µl protein solution with 1 µl reservoir solution (0.1 *M* HEPES pH 7.5, 1.5 *M* lithium sulfate) at 298 K.

2.6. X-ray diffraction data collection and processing

Crystals were harvested using a nylon loop, cryoprotected in 0.1 *M* HEPES pH 7.5, 1.5 *M* lithium sulfate, 10% ethylene glycol and then subsequently flash-cooled in liquid nitrogen. Crystals were shipped to the Advanced Photon Source, where diffraction data were collected remotely at 100 K using a MAR Mosaic 300 detector on beamline 23-ID-B (GM/CA CAT). Data were collected using an X-ray wavelength of 1.033 Å, a crystal-to-detector distance of 248 mm and a φ range of 148.5° in 0.55° increments, with 1 s exposure per frame. Data were indexed, integrated and scaled using *CCP*4 (Winn *et al.*, 2011).

2.7. Structure solution and refinement

ecSK I in the absence of bound substrate (PDB entry 1kag; Romanowski & Burley, 2002) was used as the search model for molecular replacement using *MOLREP* (Vagin & Teplyakov, 2010) to obtain initial phasing. Several regions, including the LID domain, were disordered in PDB entry 1kag and hence were absent from the search model. The resulting model was refined using *PHENIX* (Adams *et al.*, 2010), including riding H atoms to improve geometry and minimize clashes and TLS refinement to model anisotropic displacements. Manual model building and analysis was performed using *Coot* (Emsley *et al.*, 2010). Structure analysis and validation made use of *PyMOL* (Schrödinger), *PHENIX* (Adams *et al.*, 2010) and the validation tools present in the wwPDB Deposition Tool (http://deposit.wwpdb.org/deposition).

2.8. Statistical analyses

In vivo essentiality data are presented as mean ± standard error of the mean. *P*-values of less than 0.05/*N* (where *N* is the the number of comparisons) are considered to be statistically significant based on the Bonferroni correction for multiple comparisons. To normalize *in vivo* growth and survival data, $\log_{10}$-transformed values were utilized, the area under each curve was calculated and these areas were compared using two-tailed unpaired *t*-tests (*GraphPad Prism*, GraphPad Software Inc.).

3. Results and discussion

3.1. *In vivo* essentiality

The *A. baumannii* genes *aroA* and *aroC* encoding the two enzymes immediately downstream of SK in the shikimate pathway, PSCVT and CS, respectively, were previously determined to be essential *in vivo* (Umland *et al.*, 2012). It was hypothesized that *A. baumannii aroK*, encoding abSK, would be also essential *in vivo*. The *in vivo* growth and survival of the *aroK* deletion mutant AB307Δ*aroK* and its wild-type parent AB307-0294 were compared in the established rat soft-tissue infection model (Fig. 1). As expected, the wild-type parent AB307-0294 grew by ∼2 log units over 48 h. By contrast, AB307Δ*aroK* underwent complete killing over the same period. Importantly, AB307Δ*aroK* is capable of growth in rich laboratory medium, with an initial growth lag but a similar log-phase growth and plateau cell density as AB307-0294, thereby excluding a generalized growth defect.

A search of the DEG Database of Essential Genes v.11.0 (Luo *et al.*, 2014) revealed that only 11 of the 34 (32%) prokaryote genome-wide essentiality screens annotated an SK homolog as essential (Supplementary Table S1). Importantly, most of the essentiality screens cataloged within DEG were conducted *in vitro* using rich laboratory media *versus in vivo* screening or verification employing an animal infection model. A notable hit was the SK from the nonpathogenic species *A. baylyi*, as this essentiality screen was conducted on minimal laboratory medium in order to mimic the diminished nutrients present in its natural soil environment. Thus, the determination that abSK is essential *in vivo* using a rat soft-tissue infection model but non-essential on a rich laboratory medium underscores the necessity for the appropriate design and interpretation of essentiality assays.

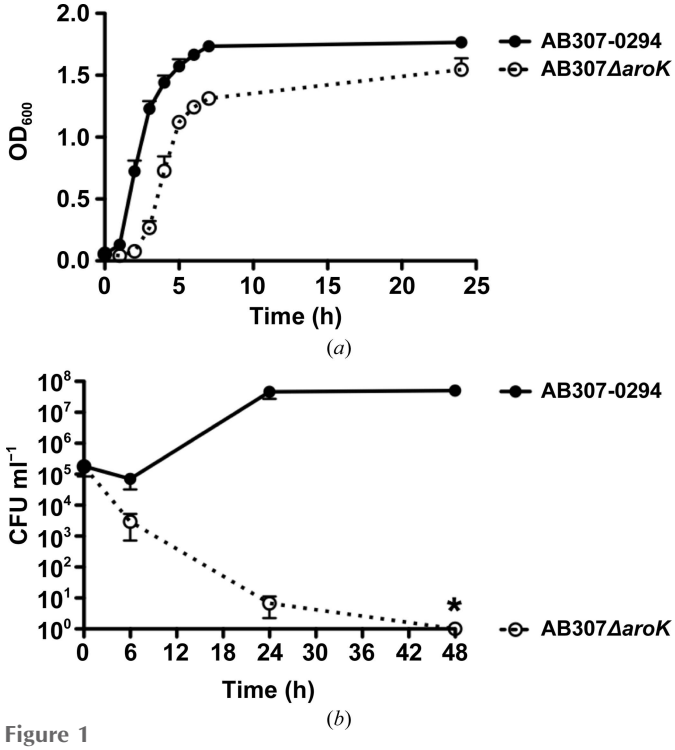

Figure 1
The growth and survival of AB307Δ*aroK* is significantly decreased compared with its wild-type parent AB307-0294 in the rat soft-tissue infection model. (*a*) Comparison of AB307-0294 and AB307Δ*aroK* growth in LB medium, as measured by optical density at 600 nm on four replicate cultures per strain. (*b*) Rats underwent challenge with either wild-type AB307-0294 or AB307Δ*aroK* to result in 1.8×10^5 CFU ml^{-1} in a pre-formed, subcutaneous, fluid-filled walled-off space. Fluid aliquots were removed at 1 min and 6, 24 and 48 h and bacterial CFU were enumerated *via* tenfold serial dilution. Data are the mean ± standard error of the mean for $n = 4$. The asterisk indicates $P < 0.0001$ (two-tailed unpaired *t*-tests) for AB307-0294 compared with AB307Δ*aroK*.

3.2. abSK enzyme kinetics

The SK shikimate-binding site has been proposed as a more promising target for drug design than its ATP-binding site owing to the diminished likelihood of activity towards off-targets. Moreover, the two SK paralogs expressed by *E. coli*, ecSK I (*aroK*-encoded) and ecSK II (*aroL*-encoded), exhibit strikingly different K_m values for shikimate: 20 m*M* and 200 µ*M*, respectively (DeFeyter & Pittard, 1986). Thus, enzyme kinetic parameters for abSK and its shikimate substrate were determined. Nonlinear regression analysis of initial velocity measurements *versus* shikimate concentration indicated the presence of modest substrate inhibition at high levels of shikimate, with $V_{max} = 1.07 \pm 0.05$ µmol s^{-1}, $k_{cat} = 21.4$ s^{-1}, $K_m = 147 \pm 15$ µ*M* and $K_i = 4950 \pm 925$ µ*M* (K_i is the dissociation constant for the substrate-inhibited complex), with $R^2 = 0.99$ (Supplementary Fig. S2). By contrast, nonlinear regression analysis assuming conventional Michaelis–Menten kinetics yielded a poor fit to the data ($R^2 = 0.81$). The abSK kinetic parameters are generally comparable to published values for other bacterial SKs, including the *aroL*-encoded *Dickeya chrysanthemi* SK. The key exception is comparison to ecSK I, which exhibits a shikimate K_m that is >100-fold larger, as noted above. Previously, it had been speculated that *aroL*-encoded SK II may generally have a greater affinity for shikimate than *aroK*-encoded enzymes, based on comparison of ecSK I and ecSK II (DeFeyter & Pittard, 1986; Rosado *et al.*, 2013). However, as kinetic parameters for more bacterial SKs are reported, the *E. coli* SK I K_m may be an outlier rather than being indicative of a simple *aroL versus aroK* categorization. Reported kinetic data for other bacteria expressing both SK I and SK II are currently lacking, so the significance of the atypical ecSK I K_m value is not yet fully resolved.

3.3. abSK–shikimate–SO_4^{2-} crystal structure overview

Recombinant abSK production in *E. coli* followed routine protocols. Sample fractions that eluted as expected for a monomer of 21.5 kDa on SEC were used in all experiments. The resulting purified abSK was >95% pure by SDS–PAGE and corresponded to the wild-type sequence (189 residues) plus a single extra vector-derived N-terminal residue (histidine) that remained following Ulp1 protease cleavage of the His_6-SUMO affinity tag. Prior to screening for initial crystallization conditions *via* the microbatch-under-oil method, known ligands (shikimate, a substrate; ADP, a product; and Mg^{2+}, a cofactor) were added to the protein sample. Following crystallization optimization, crystals of up to 0.6 × 0.4 ×

Table 1
X-ray data-collection and refinement statistics.

Values in parentheses are for the highest resolution shell.

PDB code	4y0a
Data collection	
Space group	$I2_12_12_1$
Unit-cell parameters (Å)	a = 82.0, b = 85.8, c = 112.7
Completeness (%)	98.2 (96.9)
Resolution range (Å)	36.02–1.91 (2.01–1.91)
Total No. of reflections	187575
No. of unique reflections	30525 (4303)
Multiplicity	6.1 (6.1)
R_{merge}†	0.072 (0.436)
R_{meas}‡	0.080 (0.476)
$R_{p.i.m.}$§	0.032 (0.190)
$\langle I/\sigma(I)\rangle$	12.9 (3.3)
Wilson B factor (Å^2)	32.3
Refinement	
Resolution range (Å)	36.0–1.91 (1.98–1.91)
Completeness (%)	98.0 (96.2)
No. of reflections, working set	29017
No. of reflections, test set	1507
R_{cryst}/R_{free}¶	0.1915 (0.2498)/0.2353 (0.2909)
No. of non-H atoms	
Protein	1436
Ligand + ion	27
Water	160
Model geometry (r.m.s. deviations from ideal)	
Bonds (Å)	0.021
Angles (°)	1.70
Average B factors (Å^2)	
Protein	41.3
Ligand + ion	44.0
Water	49.7
Ramachandran plot†† (%)	
Favoured	98.9
Allowed	1.1
Outliers	0
MolProbity clashscore††	1.69
Rotamer outliers†† (%)	1.3

† $R_{merge} = \sum_{hkl}\sum_i |I_i(hkl) - \langle I(hkl)\rangle| / \sum_{hkl}\sum_i I_i(hkl)$. ‡ $R_{meas} = \sum_{hkl}\{N(hkl)/[N(hkl)-1]\}^{1/2}\sum_i |I_i(hkl) - \langle I(hkl)\rangle| / \sum_{hkl}\sum_i I_i(hkl)$. § $R_{p.i.m.} = \sum_{hkl}\{1/[N(hkl)-1]\}^{1/2}\sum_i |I_i(hkl) - \langle I(hkl)\rangle| / \sum_{hkl}\sum_i I_i(hkl)$. ¶ R_{cryst} or $R_{free} = \sum_{hkl} ||F_{obs}| - |F_{calc}|| / \sum_{hkl} |F_{obs}|$ using the working or the test data sets, respectively. †† As calculated by *MolProbity*; the *MolProbity* clashscore corresponds to the 100th percentile (*i.e.* the best) among structures of comparable resolution.

0.3 mm in size were obtained in one to two weeks. Initial phasing was accomplished by molecular replacement (MR), for which unambiguous rotation and translation solutions were obtained. Importantly, the electron-density map calculated from the initial MR-derived phases included density for abSK residues (for example the LID domain) that were not present in the MR search model, suggesting that a correct solution had been identified. Statistics of the X-ray diffraction data and the final refined structure are presented in Table 1.

The overall abSK structure (Figs. 2*a* and 2*b*) is similar to those of other bacterial SKs, with a $\alpha\beta\alpha$ fold containing a central sheet of five parallel β-strands characteristic of the nucleoside monophosphate (NMP) kinase family. While the complete abSK polypeptide chain was crystallized, electron density was only observed for residues 11–189, with the N-terminus disordered. These disordered abSK N-terminal residues extend from the globular portion of the protein and are absent in many bacterial SK sequences. Residues near the C-terminus (Ser185–Lys189) possess higher than average B factors, but sufficient electron density was present for these residues to be included in the model. This abSK structure contains a bound shikimate substrate. In addition, the structure contains 160 water molecules and three SO_4^{2-} ions, including one bound to the conserved Walker A motif (or the P-loop; residues Gly25–Thr32), where it mimics the binding interactions that are expected for the β-phosphate of the ATP substrate or the ADP product. Other conserved SK structural motifs within abSK include the shikimate-binding (SB) domain (Ser49–Glu77), the Walker B motif (Val91–Gly97), the LID domain (Tyr129–Pro142), the adenine-binding loop (Ile165–Ala172) and the core domain (Pro11–Val23, Thr33–Asp48, Thr78–Leu90, Ala98–Thr128 and Glu143–Lys189). The consensus SK Walker B motif is *hhhh*GGG (Val91-Leu92-Ala93-Thr94-Gly95-Gly96-Gly97 in abSK), which differs from the conventional Walker B consensus *hhhh*D or *hhhh*DE, where *h* is a hydrophobic residue (Hanson & Whiteheart, 2005). The absent acidic residue(s) in the abSK Walker B motif is compensated by a spatially nearby DS/TD motif (Asp48-Ser49-Asp50 in abSK) that is conserved in bacterial SKs. Notably, a Mg^{2+} ion was not observed bound in the expected location coordinated to the hydroxyl O atom of Thr32, despite the addition of $MgCl_2$ to the abSK sample. This absence may be a result of the high ionic strength used for crystallization.

3.4. abSK ligand binding

abSK was co-crystallized with the substrate shikimate, which was well defined by $F_o - F_c$ electron density in the partially refined structure. Shikimate was subsequently included in the model and refined, and was finally verified with a simulated-annealing OMIT map (Fig. 2*c*). The overall shikimate-binding site is similar to those in previously reported SK structures. Several polar interactions orientate shikimate: a salt bridge between Arg153 (core domain) and the carboxyl group of shikimate, a second salt bridge between Arg74 (SB domain) and the same carboxyl group, two hydrogen bonds between the Asp50 side-chain carboxyl (SB domain) and the hydroxyl group attached to each of the C6 and C8 atoms of shikimate, and a hydrogen bond between the main-chain amide of Gly96 (Walker B) and the hydroxyl group attached to the C9 atom of shikimate. Protein–shikimate hydrophobic and van der Waals interactions occur for residues present in the P-loop (Met27), the SB domain (Ile61 and Phe73), the Walker B motif (Gly95 and Gly97) and the LID domain (Pro135 and Leu136).

Five well ordered waters participate in bridging interactions between abSK and shikimate (Table 2 and Fig. 2*c*). The majority of these bridging waters have been observed in other bacterial SK crystal structures that include bound shikimate, suggesting that they play an inherent role in the binding-site architecture (Blanco *et al.*, 2013). For example, the crystal structure of *Mycobacterium tuberculosis* SK (mtSK) co-crystallized with shikimate and a sulfate ion (PDB entry 2iyx; Hartmann *et al.*, 2006) possesses four of the five bridging waters observed in abSK. Interestingly, the sole exception, corresponding to abSK water 17, is absent in mtSK owing to a

Table 2
Waters involved in bridging interactions between abSK and shikimate.

Bridging water	Shikimate	abSK
Water 2	O12	Arg74 $N^{\eta1}$, Glu77 $O^{\varepsilon2}$, Gly97 N
Water 3	O7	Asn133 O
Water 6	O11	Lys31 N^{ζ}, Arg134 $N^{\eta1}$
Water 8	O7	Leu136 N
Water 17	O2	Met27 N, Arg153 $N^{\eta1}$

nonconserved residue lining the respective shikimate-binding sites (Fig. 3). In abSK, water 17 hydrogen bonds to the main-chain amide of Met27, the side chain of which also contacts shikimate. In mtSK, the corresponding residue position is occupied by Pro11, which lacks the ability to form a main-chain amide hydrogen bond. The presence of the larger methionine residue in the shikimate-binding site of abSK decreases the cavity volume compared with that in mtSK. In fact, mtSK possesses an additional water molecule in place of the Met27 side chain in abSK. The respective abSK and mtSK shikimate-binding sites are differentiated by both amino-acid composition and water structure. Given that the shikimate-binding mode is highly similar in both abSK and mtSK, and the respective K_m values (abSK, 147 ± 15 μ*M*; mtSK, 650 ± 28 μ*M* or 410 ± 20 μ*M*; Gu *et al.*, 2002; Rosado *et al.*, 2013) are comparable, these differences have at best a modest effect upon shikimate binding. However, these differences may be exploited during the development of narrow-spectrum antibiotics, or should be considered during broad-spectrum antibiotic design.

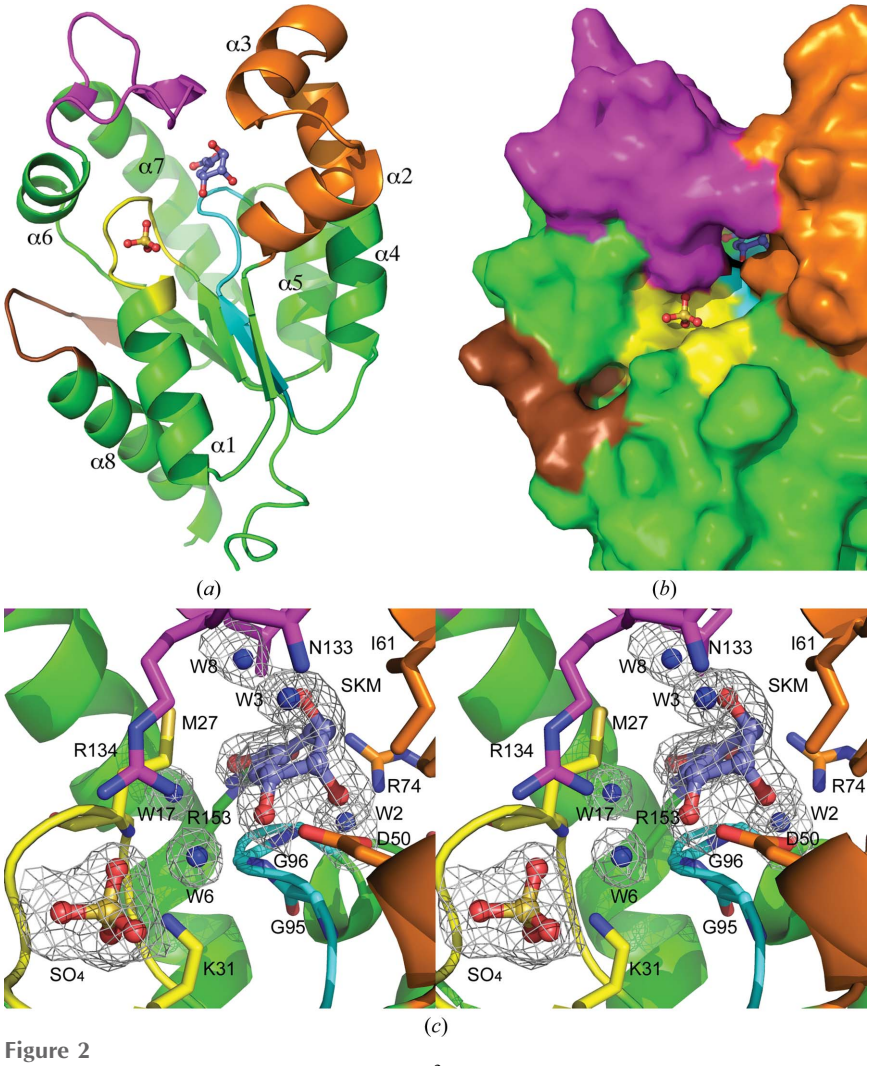

Figure 2
Crystal structure of the abSK–shikimate–SO_4^{2-} complex. (*a*) abSK displayed as a ribbon cartoon, with bound shikimate and the SO_4^{2-} ion interacting with the P-loop displayed as ball-and-stick models. (*b*) A surface representation of abSK zoomed in on the bound ligands. Shikimate is almost completely buried by the closed LID conformation. (*c*) Stereoview of the abSK active site with corresponding electron density for bound ligands and waters. The $F_o - F_c$ simulated-annealing OMIT electron-density map is contoured at 3σ around shikimate (medium blue C atoms), bridging waters (blue spheres) and SO_4^{2-} (yellow S atoms) bound to the P-loop. The abSK orientation is identical across images, and important functional motifs are color-coded: core domain, green; Walker A motif (P-loop), yellow; Walker B motif, cyan; shikimate-binding domain, orange; adenine-binding loop, brown; LID, magenta.

A second example of the lack of conservation within the shikimate-binding site is SK II (*aroL*-encoded) from *Dickeya chrysanthemi* (reclassified from *Erwinia chrysanthemi*; PDB entry 1shk; dcSK; Krell *et al.*, 1997). *D. chrysanthemi* is a plant pathogen belonging to the Enterobacteriaceae family and is closely related to a number of important human pathogens. It also illustrates the small but important number of bacterial pathogens (for example *E. coli*, *Salmonella typhimurium* and *Yersinia pestis*) that possess two SK paralogs encoded by *aroK* and *aroL* genes. The dcSK residue corresponding to Leu136 in abSK is Thr122, resulting in both a change in volume and hydrophobicity in the respective shikimate-binding sites. Other *aroL*-encoded SK II enzymes generally contain a threonine or a serine at this position *versus* a leucine in *aroK*-encoded SKs (Supplementary Fig. S3). A second differentiator between *aroK*-encoded and *aroL*-encoded SK paralogs is at the position corresponding to Met27 in abSK. This position is a conserved methionine in most *aroK*-encoded SKs, while this position is typically an arginine in *aroL*-encoded enzymes (for example Arg11 in dcSK). mtSK is an important exception to this trend, with a proline (Pro11) at this site, as previously discussed. The effect of the differences between abSK and SK II upon shikimate binding appears to be modest, as the K_m values are similar (ecSK II, 200 μ*M*; dcSK, 310 μ*M*; DeFeyter & Pittard, 1986; Krell *et al.*, 2001), as is the overall binding mode. However, these differences may be important during the design of inhibitors with varying levels of SK I or SK II specificity.

ADP was included in the abSK crystallization mother liquor, but was not observed

in the electron density despite the binding site being intact. This observation is likely to be explained by the SO_4^{2-} ion, which is present at high concentration in the crystallization cocktail, binding to the P-loop and thereby blocking binding interactions with the β-phosphate of ADP. The adenine-binding loop exhibits significant sequence variability, with none of the residues fully conserved across abSK plus the eight other bacterial SKs currently represented in the PDB. Proposed consensus sequences for this motif include V/I-D-A-*X*-Q/N-*X*-P (Romanowski & Burley, 2002) and V/I-D-*X*-*X*-*X*-*X*-(*X*)-P (Gu *et al.*, 2002). In abSK, the sequence of this motif sequence is Ile165-Glu166-Thr167-Asn168-Gln169-Gly170-Ala171-Ala172, which deviates significantly from the suggested consensus sequences (Moodie *et al.*, 1996). The abSK adenine-binding loop main chain was well resolved in electron density, but the *B* factors were generally larger than average. An opening of the abSK adenine-binding loop is likely to occur upon ATP or ADP binding, as the main-chain atoms of residues Gln169 and Gly170 impinge upon the expected binding site.

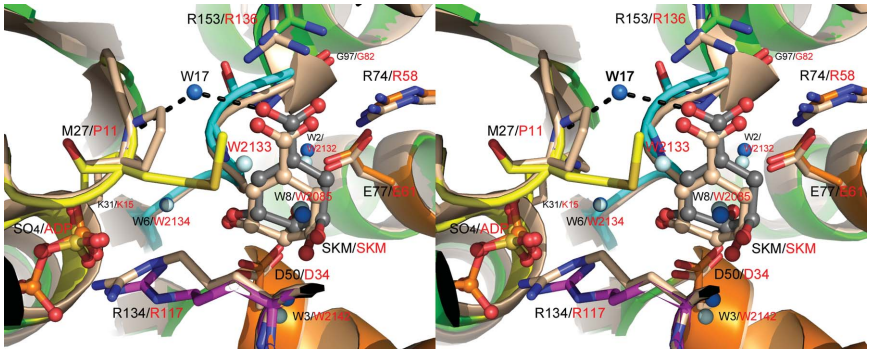

Figure 3
A nonconserved residue differentiates the abSK and mtSK shikimate-binding pockets, which may impact on SK inhibitor design. A stereoview of the mtSK–shikimate–ADP ternary complex (PDB entry 2iyq; light tan ribbon and C atoms, light cyan waters, red residue labels) superimposed upon the abSK–shikimate–SO_4^{2-} ternary complex (gray shikimate C atoms, blue waters, black residue labels and functional motifs color-coded as in Fig. 2). The side chain of Met27 of abSK directly contacts shikimate and participates in a bridging water (water 17) interaction with shikimate through its main-chain amide. mtSK has a proline residue (Pro11) in place of Met27 of abSK, thus altering the shikimate-binding site and associated bound waters. Specifically, mtSK lacks a bridging water corresponding to water 17 in abSK, but has an extra water (water 2133) that occupies the volume filled by the side chain of Met27 of abSK.

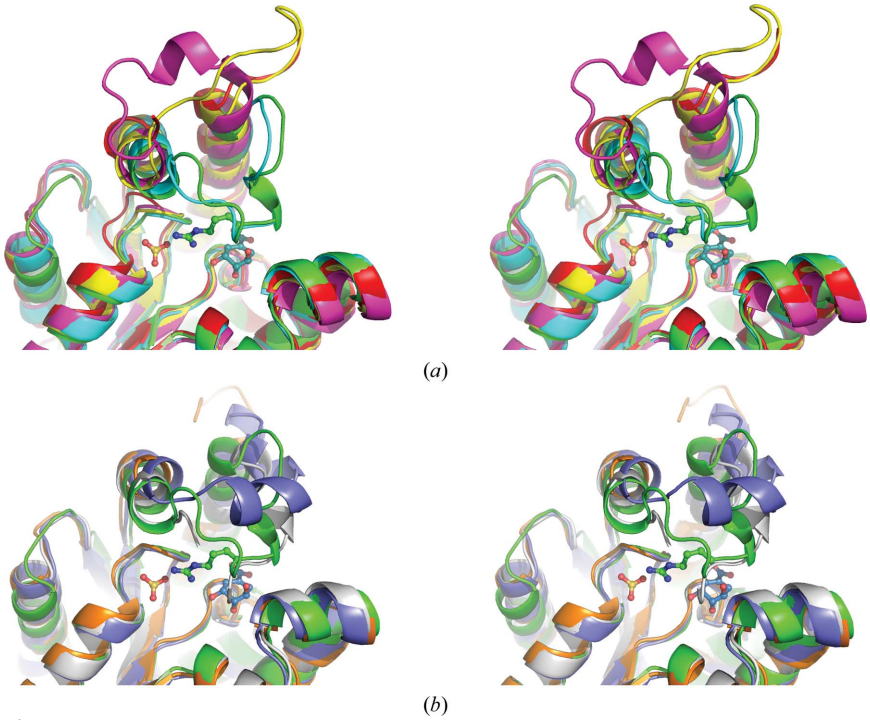

Figure 4
Stereoview comparison of the open and closed conformations of the SK LID domain. (*a*) abSK (green) superimposed with selected mtSK structures, illustrating induced-fit conformation differences: PDB entry 2iyq, cyan (closed); PDB entry 2iyu, magenta (open); PDB entry 2iyw, yellow (open); PDB entry 2g1j, red (open, disordered LID). (*b*) abSK (green) superimposed with selected *H. pylori* SK structures: PDB entry 1zui, light gray (closed with partially disordered LID); PDB entry 3n2e, blue (partially closed); PDB entry 3hr7, orange (open, disordered LID). Arg118 of abSK plus the abSK ligands (shikimate and SO_4^{2-} interacting with the P-loop) are displayed in ball-and-stick representation. Smaller conformational shifts are observed for the adenine-binding loop and SB domain.

3.5. SK conformational flexibility

As described above, the overall three-dimensional structure of abSK was consistent with the other previously reported SK homolog crystal structures (a total of 36 entries in the PDB as of 17 March 2015, representing homologs from nine distinct species). Pairwise r.m.s.d. values (C^{α} atoms) calculated by *DALI* (Holm & Park, 2000) for abSK superimposed against each deposited SK crystal structure resulted in a best overall structural agreement of 1.3 Å with two mtSK structures (PDB entries 2iyq and 2dfn; 165 superimposed residues at 38% sequence identity; Hartmann *et al.*, 2006; Dias *et al.*, 2007) and a maximum difference of 2.5 Å for two mtSK structures (PDB entries 2iys and 2iyt; 175 superimposed residues at 37% sequence identity; Hartmann *et al.*, 2006). Superposition of abSK and a dcSK K15M mutant (PDB entry 1e6c; 158 superimposed residues at 35% sequence identity; Krell *et al.*, 2001) yielded a larger r.m.s.d. of 2.7 Å, but the mutation structurally perturbed the protein.

The previously reported crystal structures of bacterial SKs revealed significant conformational flexibility correlated to the presence of bound ligand (Blanco *et al.*, 2013; Cheng *et al.*, 2012; Dhaliwal *et al.*, 2004; Gu *et al.*, 2002; Hartmann *et al.*, 2006). This induced-fit conformational change is the basis for mtSK exhibiting both the minimum and maximum structural alignment r.m.s.d. values to the abSK crystal

structure. mtSK has been extensively studied crystallographically bound to a variety of ligands. The LID region (abSK residues Tyr129–Pro142) exhibits the largest conformational change, from an open form in the absence of shikimate or ATP (or mimics thereof) to a closed form upon shikimate or ATP ligand binding. The LID domain in the abSK crystal structure is in a closed conformation, presumably owing to the presence of bound shikimate and the SO_4^{2-} ion bound to the P-loop. Ligand binding is thought to occur in a random order, displaying synergic binding coupled with the significant SK conformational changes triggered upon binding of either substrate (Hartmann *et al.*, 2006; Krell *et al.*, 2001; Rosado *et al.*, 2013). Shikimate binding to abSK involves interactions with multiple regions of the enzyme, including the LID, core, SB, Walker A (P-loop) and Walker B motifs. Thus, it is not surprising that significant conformation shifts, primarily an overall compaction, occur upon shikimate binding. The closed LID of abSK, with only bound shikimate and an SO_4^{2-} ion mimicking phosphate, does not obscure the ATP-binding site from access from the bulk solution (Fig. 2*b*). Rather, the closed LID forms an ATP-binding cleft that will protect the nucleoside triphosphate upon binding. In addition to the interaction of abSK LID residue Arg134 with shikimate through a bridging water, it forms a salt bridge to the P-loop-bound SO_4^{2-} and presumably participates in a similar interaction with the β-phosphate of a bound ATP or ADP (Figs. 2*c* and 3). A comparable role for analogous LID arginine residues has been observed in other SK structures postulated to stabilize the pentavalent phosphorus transition-state intermediate (Gan *et al.*, 2006).

There appears to be no canonical open or closed LID conformation, but rather general structural trends (Fig. 4). In part, this may be owing to sequence variability in the LID region across SK homologs (Supplementary Figs. S1 and S3). The distinctly different observed open LID conformations plus the occurrence of partially or fully disordered LIDs indicate high mobility of this region in the absence of both shikimate and ATP/ADP. It is not surprising that there may not be a consensus open LID conformation across the SK family, as the purpose of the open LID is to allow ingress or egress from the ligand-binding sites. LIDs in the closed form display less severe structural differences owing to the functional requirement of shielding the shikimate-binding site plus participating in forming the ATP-binding cleft. The most conserved structural element of the closed LID is the arginine (Arg134 in abSK) positioned such that its guanidino group interacts with both the β-phosphate of ATP or ADP (or SO_4^{2-} mimicking phosphate) and shikimate. Similar LID conformations (*e.g.* abSK and mtSK; PDB entry 2iyq) still display structural diversity, with the corresponding C^{α} atoms of superimposed LIDs differing by up to 3.5 Å (Val139 in abSK and Gly122 in mtSK), while being most similar (0.32 Å) at the conserved and catalytically important arginine (Arg134 in abSK and Arg117 in mtSK). By comparison, the distance between the respective C^{α} atoms of Arg134 in abSK and Arg117 in mtSK is 24.5 Å for abSK superimposed upon mtSK with an open LID conformation (PDB entry 2iyu).

Other regions of SK exhibit smaller conformational shifts upon ligand binding (Gu *et al.*, 2002; Cheng *et al.*, 2012). Comparison of the abSK–shikimate–SO_4^{2-} complex with uncomplexed and ligand-bound SK homologs suggests that these smaller ligand-induced conformational changes also occur within abSK. In particular, the abSK SB domain and each of the core α-helices flanking the ends of the LID shift to form a more compact globular structure upon shikimate binding (Fig. 4). Conversely, the abSK–shikimate–SO_4^{2-} complex adenine-binding loop must open up somewhat upon ATP binding, as otherwise a number of energetically unfavorable protein–ligand clashes would occur based upon the expected ATP-binding interaction.

4. Conclusion

The determination that abSK is *in vivo* essential in *A. baumannii* expands the set of pathogenic bacteria in which SK may serve as a useful target for new antibiotic development to combat the ever-increasing incidence of MDR and XDR clinical isolates (>50% in some US intensive care units; Lee *et al.*, 2014). The crystal structure of the abSK–shikimate–SO_4^{2-} complex adds to the structural catalog of members of the SK family from bacterial pathogens or close relatives. While the SK family exhibits a common fold and similar functional motifs, sufficient primary and tertiary structural diversity exists between the members to impact the development and optimization of both broad- and narrow-spectrum antibiotics. Moreover, the large induced-fit conformational changes that occur upon ATP and shikimate substrate binding place great importance on defining these conformational shifts for specific SK homologs of interest. In particular, the shikimate-binding site has been suggested as a preferred targeting site for inhibitor or antibiotic development in order to design enzyme specificity into the drug. The highly flexible LID region participates in the formation of the shikimate-binding site, and the LID sequence and structure differs across SK homologs. An additional appeal of focusing antibiotic development on the SK shikimate-binding site is to enable the development of a multi-target drug. Antibiotics effective against multiple targets promise to have a decreased rate of development of resistant strains (Silver, 2007). The three consecutive terminal enzymes of the shikimate pathway (*i.e.* SK, PSCVT and CS) all utilize a substrate based upon a similar core scaffold, and hence may share a number of similar binding determinates that can be exploited to develop a single small-molecule therapeutic that is active against all three targets.

Acknowledgements

This work was supported in part by Telemedicine and Advanced Technical Research Center (TATRC) Cooperative Agreement W23RYX1055N607 (TAR, LWS and TCU), an Interdisciplinary Grant from the University at Buffalo (TAR and TCU) and a VA Merit Review grant from the Department of Veterans Affairs (TAR). We wish to thank Ms Hannah Brummer for assistance in expression vector and abSK protein production. The Ulp1 protease expression vector was a kind

gift from Dr Christopher Lima (Sloan–Kettering Institute). This research used the resources of the Advanced Photon Source (APS), a US Department of Energy (DOE) Office of Science User Facility operated for the DOE Office of Science by Argonne National Laboratory under Contract No. DE-AC02-06CH11357. We thank the staff at APS beamline 23-ID-B (GM/CA CAT) for assistance in X-ray diffraction data collection.

References

Abell, C. (1999). *Comprehensive Natural Products Chemistry*, edited by O. Meth-Cohn, D. Barton & K. Nakanishi, pp. 573–607. Oxford: Pergamon Press.

Adams, P. D. *et al.* (2010). *Acta Cryst.* D**66**, 213–221.

Adams, M. D., Goglin, K., Molyneaux, N., Hujer, K. M., Lavender, H., Jamison, J. J., MacDonald, I. J., Martin, K. M., Russo, T., Campagnari, A. A., Hujer, A. M., Bonomo, R. A. & Gill, S. R. (2008). *J. Bacteriol.* **190**, 8053–8064.

Bentley, R. & Haslam, E. (1990). *Crit. Rev. Biochem. Mol. Biol.* **25**, 307–384.

Blanco, B., Prado, V., Lence, E., Otero, J. M., Garcia-Doval, C., van Raaij, M. J., Llamas-Saiz, A. L., Lamb, H., Hawkins, A. R. & González-Bello, C. (2013). *J. Am. Chem. Soc.* **135**, 12366–12376.

Boucher, H. W., Talbot, G. H., Benjamin, D. K. Jr, Bradley, J., Guidos, R. J., Jones, R. N., Murray, B. E., Bonomo, R. A. & Gilbert, D. (2013). *Clin. Infect. Dis.* **56**, 1685–1694.

Brinster, S., Lamberet, G., Staels, B., Trieu-Cuot, P., Gruss, A. & Poyart, C. (2009). *Nature (London)*, **458**, 83–86.

Brinster, S., Lamberet, G., Staels, B., Trieu-Cuot, P., Gruss, A. & Poyart, C. (2010). *Nature (London)*, **463**, E4.

Cheng, W.-C., Chen, Y.-F., Wang, H.-J., Hsu, K.-C., Lin, S.-C., Chen, T.-J., Yang, J.-M. & Wang, W.-C. (2012). *PLoS One*, **7**, e33481.

Coggins, J. R., Abell, C., Evans, L. B., Frederickson, M., Robinson, D. A., Roszak, A. W. & Lapthorn, A. P. (2003). *Biochem. Soc. Trans.* **31**, 548–552.

DeFeyter, R. C. & Pittard, J. (1986). *J. Bacteriol.* **165**, 331–333.

Dhaliwal, B., Nichols, C. E., Ren, J., Lockyer, M., Charles, I., Hawkins, A. R. & Stammers, D. K. (2004). *FEBS Lett.* **574**, 49–54.

Dias, M. V. B., Faím, L. M., Vasconcelos, I. B., de Oliveira, J. S., Basso, L. A., Santos, D. S. & de Azevedo, W. F. (2007). *Acta Cryst.* F**63**, 1–6.

Emsley, P., Lohkamp, B., Scott, W. G. & Cowtan, K. (2010). *Acta Cryst.* D**66**, 486–501.

Fahnoe, K. C., Flanagan, M. E., Gibson, G., Shanmugasundaram, V., Che, Y. & Tomaras, A. P. (2012). *PLoS One*, **7**, e51732.

Gan, J., Gu, Y., Li, Y., Yan, H. & Ji, X. (2006). *Biochemistry*, **45**, 8539–8545.

Gu, Y., Reshetnikova, L., Li, Y., Wu, Y., Yan, H., Singh, S. & Ji, X. (2002). *J. Mol. Biol.* **319**, 779–789.

Hanson, P. I. & Whiteheart, S. W. (2005). *Nature Rev. Mol. Cell Biol.* **6**, 519–529.

Hartmann, M. D., Bourenkov, G. P., Oberschall, A., Strizhov, N. & Bartunik, H. D. (2006). *J. Mol. Biol.* **364**, 411–423.

Haslam, E. (1974). *The Shikimate Pathway*, edited by E. Haslam, pp. 128–185. London: Butterworth–Heinemann.

Herrmann, K. M. & Weaver, L. M. (1999). *Annu. Rev. Plant Physiol. Plant Mol. Biol.* **50**, 473–503.

Holm, L. & Park, J. (2000). *Bioinformatics*, **16**, 566–567.

Hsu, K.-C., Cheng, W.-C., Chen, Y.-F., Wang, W.-C. & Yang, J.-M. (2013). *PLoS Comput. Biol.* **9**, e1003127.

Krell, T., Coyle, J. E., Horsburgh, M. J., Coggins, J. R. & Lapthorn, A. J. (1997). *Acta Cryst.* D**53**, 612–614.

Krell, T., Maclean, J., Boam, D. J., Cooper, A., Resmini, M., Brocklehurst, K., Kelly, S. M., Price, N. C., Lapthorn, A. J. & Coggins, J. R. (2001). *Protein Sci.* **10**, 1137–1149.

Lee, H.-Y., Chen, C.-L., Wu, S.-R., Huang, C.-W. & Chiu, C.-H. (2014). *Crit. Care Med.* **42**, 1081–1088.

Luft, J. R., Collins, R. J., Fehrman, N. A., Lauricella, A. M., Veatch, C. K. & DeTitta, G. T. (2003). *J. Struct. Biol.* **142**, 170–179.

Luke, N. R., Howlett, A. J., Shao, J. & Campagnari, A. A. (2004). *Infect. Immun.* **72**, 6262–6270.

Luo, H., Lin, Y., Gao, F., Zhang, C.-T. & Zhang, R. (2014). *Nucleic Acids Res.* **42**, D574–D580.

McConkey, G. A., Pinney, J. W., Westhead, D. R., Plueckhahn, K., Fitzpatrick, T. B., Macheroux, P. & Kappes, B. (2004). *Trends Parasitol.* **20**, 60–65.

McLeod, R., Roberts, F., Roberts, C. W., Johnson, J. J., Kyle, D. E., Krell, T., Coggins, J. R., Coombs, G. H., Milhous, W. K., Tzipori, S., Ferguson, D. J. P. & Chakrabarti, D. (1998). *Nature (London)*, **393**, 801–805.

Millar, G., Lewendon, A., Hunter, M. G. & Coggins, J. R. (1986). *Biochem. J.* **237**, 427–437.

Moodie, S. L., Mitchell, J. B. O. & Thornton, J. M. (1996). *J. Mol. Biol.* **263**, 486–500.

Mossessova, E. & Lima, C. D. (2000). *Mol. Cell*, **5**, 865–876.

Perros, M. (2015). *Science*, **347**, 1062–1064.

Rogers, S. G., Brand, L. A., Holder, S. B., Sharps, E. S. & Brackin, M. J. (1983). *Appl. Environ. Microbiol.* **46**, 37–43.

Romanowski, M. J. & Burley, S. K. (2002). *Proteins*, **47**, 558–562.

Rosado, L. A., Vasconcelos, I. B., Palma, M. S., Frappier, V., Najmanovich, R. J., Santos, D. S. & Basso, L. A. (2013). *PLoS One*, **8**, e61918.

Russo, T. A., Luke, N. R., Beanan, J. M., Olson, R., Sauberan, S. L., MacDonald, U., Schultz, L. W., Umland, T. C. & Campagnari, A. A. (2010). *Infect. Immun.* **78**, 3993–4000.

Russo, T. A., MacDonald, U., Beanan, J. M., Olson, R., MacDonald, I. J., Sauberan, S. L., Luke, N. R., Schultz, L. W. & Umland, T. C. (2009). *J. Infect. Dis.* **199**, 513–521.

Silver, L. L. (2007). *Nature Rev. Drug Discov.* **6**, 41–55.

Spellberg, B. & Bonomo, R. A. (2014). *Crit. Care Med.* **42**, 1289–1291.

Steinrücken, H. C. & Amrhein, N. (1980). *Biochem. Biophys. Res. Commun.* **94**, 1207–1212.

Umland, T. C., Schultz, L. W., MacDonald, U., Beanan, J. M., Olson, R. & Russo, T. A. (2012). *MBio*, **3**, e00113-12.

Vagin, A. & Teplyakov, A. (2010). *Acta Cryst.* D**66**, 22–25.

Winn, M. D. *et al.* (2011). *Acta Cryst.* D**67**, 235–242.